Journal of Electronic Imaging

JElectronicImaging.org

# Satellite image resolution enhancement using discrete wavelet transform and new edge-directed interpolation

Wasnaa Witwit
Yifan Zhao
Karl Jenkins
Yitian Zhao

SPIE. IS&T imaging.org

Wasnaa Witwit, Yifan Zhao, Karl Jenkins, Yitian Zhao, "Satellite image resolution enhancement using discrete wavelet transform and new edge-directed interpolation," *J. Electron. Imaging* **26**(2), 023014 (2017), doi: 10.1117/1.JEI.26.2.023014.

# Satellite image resolution enhancement using discrete wavelet transform and new edge-directed interpolation

**Wasnaa Witwit,[a] Yifan Zhao,[a,*] Karl Jenkins,[b] and Yitian Zhao[c]**
[a]Cranfield University, Through-life Engineering Services Institute, Cranfield Manufacturing, Cranfield, United Kingdom
[b]Cranfield University, Centre for Computational Engineering Sciences, Cranfield Aerospace, Cranfield, United Kingdom
[c]Beijing Institute of Technology, School of Optics and Electronics, Beijing Engineering Research Center of Mixed Reality and Advanced Display, Beijing, China

**Abstract.** An image resolution enhancement approach based on discrete wavelet transform (DWT) and new edge-directed interpolation (NEDI) for degraded satellite images by geometric distortion to correct the errors in image geometry and recover the edge details of directional high-frequency subbands is proposed. The observed image is decomposed into four frequency subbands through DWT, and then the three high-frequency subbands and the observed image are processed with NEDI. To better preserve the edges and remove potential noise in the estimated high-frequency subbands, an adaptive threshold is applied to process the estimated wavelet coefficients. Finally, the enhanced image is reconstructed by applying inverse DWT. Four criteria are introduced, aiming to better assess the overall performance of the proposed approach for different types of satellite images. A public satellite images data set is selected for the validation purpose. The visual and quantitative results show the superiority of the proposed approach over the conventional and state-of-the-art image resolution enhancement techniques. *© 2017 SPIE and IS&T* [DOI: 10.1117/1.JEI.26.2.023014]

Keywords: discrete wavelet transform; new edge-directed interpolation; image resolution enhancement; satellite image; geometric distortion; super-resolution.

Paper 160993 received Nov. 28, 2016; accepted for publication Mar. 16, 2017; published online Mar. 30, 2017.

## 1 Introduction

Satellite imaging is usually the most cost efficient means of collecting regular and frequent data about the earth's surface. These data are routinely used to monitor land use change, urban expansion, agricultural health and productivity, the status of urban tree corridors, fire threat, environmental condition, etc.[1] High-resolution (HR) satellite images are strongly demanded in many applications, such as remote sensing, astronomy, geoscience, and geographical information systems, not only for providing better visualization but also for extracting additional information details, which can be crucial in these applications. For example, HR satellite images are crucial in distinguishing an object from similar ones and achieving a better classification of regions in a multispectral remote sensing image.[2,3]

When remote sensing image data are acquired by sensors on satellites and aircraft, the data can have errors in geometry and in the measured intensity values of the pixels. The first is referred to as geometric errors while the latter is referred to as radiometric errors.[4,5] The geometric errors can result from many sources, such as the relative motions of the remote sensing platform, nonidealities in the sensors themselves, the rotation of the earth, and uncontrolled variations in the position and attitude of the platform. However, the radiometric errors can arise from the instruments used to acquire the image data, the wavelength dependence of solar radiation, and the effect of the atmosphere. Geometric distortion effects of the image data are more severe than radiometric distortion and lead to varying degrees of severity in the produced image. Therefore, image processing procedures are used to compensate for these errors and to find more general applications. Resolution enhancement is one of the applications for correcting the errors in image geometry.[4] Resolution enhancement based on a single low-resolution (LR) image or multiple LR images, also called super-resolution (SR), recently has attracted lots of interest and has been used for different applications, such as satellite imaging,[6–8] medical imaging,[9,10] and video surveillance systems,[11] etc.

Interpolation is one of the commonly used techniques for image resolution enhancement. Fundamentally, it is a process of estimating values at unknown locations using known data.[12] There are four well-known conventional interpolation methods: nearest neighbor, bilinear, bicubic, and Lanczos. However, these linear methods cannot handle the fast growing statistics around edges and accordingly yield interpolated images with blurred edges and undesirable artifacts. To address this problem, other nonlinear interpolation-based resolution enhancement methods have been developed to improve the subjective quality by taking edge information into account, such as edge-directed interpolation (EDI)[13] and new edge-directed interpolation (NEDI).[14] EDI emphasizes the visual integrity of the edges, and NEDI is the upgraded version. Nevertheless, the improvements by these methods are limited at the textures and nonlinear edges of the interpolated images.[15] However, a lot of research has achieved enhanced performance of NEDI because the NEDI method uses a relatively simple model and hence has low computational complexity. The modified NEDI method was presented in Ref. 16 by considering a modified training

*Address all correspondence to: Yifan Zhao, E-mail: yifan.zhao@cranfield.ac.uk

widow structure to eliminate the prediction error accumulation and extending the covariance values into multiple directions to mitigate the covariance mismatch problem.

Another class of resolution enhancement methods is wavelet based. A common assumption of wavelet-based methods is that the LR image is the low-pass filtered subband of the wavelet-transformed HR image. Estimating the unknown wavelet coefficients in subbands containing high-pass frequency spatial information is the essential target of this class of algorithms to estimate the HR image from the LR image. A simple approach, called wavelet zero padding (WZP), is to recover an approximation to the HR image by filling the unknown detail wavelet coefficients with zeros and applying the inverse wavelet transform. Although this method is able to surpass the conventional interpolation methods, it commonly introduces artifacts, such as smoothing and ringing, into the reconstructed HR image.

Many advanced methods have been introduced to estimate the wavelet coefficients of high-frequency subbands. In Refs. 17 and 18, only the coefficients of high-frequency subbands with significant magnitudes were estimated as the evolution of the wavelet coefficients among the scales while it was difficult to estimate the other small coefficients. The performance is mainly affected by the signs of the estimated coefficients being copied directly from the signs of the parent coefficients without any attempt to estimate the actual signs. However, the accepted fact is that there is very low correlation between the signs of the parent coefficients and the estimated coefficients. Therefore, the signs of the estimated coefficients using extrema evolution techniques cannot be relied upon. A hidden Markov tree-based method was proposed in Ref. 19 and an extended version of this method was presented in Ref. 20, to estimate the unknown detail coefficients by the mixed Gaussian distributions, which are symmetrical around zero. These methods are used to determine the most probable state for the estimated coefficient. The performance is also affected by the sign changes between the scales not being taken into account. A nondirectional cycle-spinning (CS) technique,[21] called WZP-CS, was developed as an effective method toward reducing ringing artifacts by averaging out the translated zero-padded reconstructed images. However, ringing artifacts not only occur in the neighborhood of edges; in particular, they are predominantly correlated with the orientation of the edges. A directional CS technique, which can refine better edge orientation and prevent ringing artifacts, was introduced in Ref. 22. Additionally, it can reduce the computational complexity compared with a nondirectional CS technique. A further improvement of this method could be obtained by applying a CS and edge rectification technique.[23] Recently, a dual-tree complex wavelet transform (DT-CWT) technique[6] was proposed for resolution enhancement of satellite images. One-level DT-CWT decomposes an input LR image into different frequency subbands, and then the high-frequency subbands and the input image are interpolated using bicubic interpolation. Finally, a super-resolved image is generated by combining all these interpolated subbands through the inverse DT-CWT. More recently, a DT-CWT technique[8] based on nonlocal-means filter and Lanczos interpolation was proposed to improve the performance. In recent years, discrete wavelet transform (DWT)-based image resolution enhancement techniques have attracted increasing investigations. Acharya and Tsai[24,25] proposed using one-level DWT to separate an LR image into four frequency subbands, and then the three high-frequency subbands are upsampled by inserting zeros between successive rows and columns. An upsampled image is generated by performing the inverse DWT on these approximated subbands. Recently, a Demirel–Anbarjafari super-resolution (DASR) technique was proposed[26] in which the decomposed three high-frequency subbands and the input image were interpolated using bicubic interpolation. Upgrading from the DASR, Demirel and Anbarjafari[7] introduced a DWT-Diff method, in which the high-frequency subbands are further enhanced by considering the difference between the input LR image and the interpolated low-low (LL) subband. The same authors proposed a DWT–stationary wavelet transform (SWT) technique based on DWT and SWT,[27] which introduced an intermediate process by adding the high-frequency subbands obtained through SWT of the input image with the high-frequency subbands obtained through DWT.

This paper proposes an improved image resolution enhancement approach, called DWT-NEDI, which integrates merits from both the frequency domain and spatial domain. There are three major stages in the proposed method. First, a DWT is employed to decompose the input image into different frequency subbands in the frequency domain. Second, for the three high-frequency subbands, NEDI is employed to process each of them and output the estimated subbands using soft-thresholding. Meanwhile, the input image is directly interpolated by NEDI to output the low-frequency subband. Finally, after combining both low- and high-frequency subbands, the processed image is transformed back to the spatial domain as the outcome of resolution enhancement through inverse discrete wavelet transform (IDWT). Recently, learning-based SR methods have emerged to further boost the efficiency of single image SR. For example, Timofte et al.[28] introduced a simple function method and the anchored neighbor regression (ANR) method. The same authors further improved the ANR method and proposed the adjusted ANR ($A^+$) for fast SR.[29] These methods divide the training data into a small number of groups and learn a regression model for each group. Deep learning-based SR approaches have also appeared to improve SR results. Huang and Siu[30] proposed using a decision tree method and an SR hierarchical decision trees (SRHDT) method for improving SR performance. To better model complex image contents and details, deep learning networks methods have been introduced. Dong et al.[31] proposed an SR convolution neural network (SRCNN) method to perform a sparse reconstruction. However, this method does not exploit natural image priors and suffers from losing sharp edges. Following the SRCNN method, a deep edge-guided recurrent residual method[32] was proposed to provide high-quality image SR and recover the edges by recurrent residual learning. A limitation of learning-based methods is that they require a large amount of training data sets.

The majority of developed SR approaches focus on grayscale or single-channel image SR, while this paper applies the performance of the proposed technique to color images. Although the proposed approach also works well for other types of images, this paper focuses its application on satellite images. The paper is organized as follows. Section 2 introduces the detail of the proposed method. Results and

discussions based on testing five categories of satellite images are presented in Sec. 3, and conclusions are given in Sec. 4.

## 2 Proposed Resolution Enhancement Approach

The main drawback for using a direct interpolation to enhance image resolution is the generated visual degradations around edge areas and, as a result, the production of blurred edges. This degradation is due to annoying levels of smoothing across edges caused by the employed interpolation method, which does not use any information pertinent to the edges in the original image. Preserving the high-frequency components (i.e., edges) and consequently increasing the quality of the resulted HR image is the fundamental target for reconstructing the HR image from the given LR image.

Therefore, in this work, the DWT process was employed to isolate and preserve the edges of the image using the interpolation of high-frequency subbands. This is due to the interpolation of isolated high-frequency components in the high-frequency subbands preserving more edges of the image than interpolating the image directly. On the other hand, DWT decomposes the given image into three directional high-frequency subbands, which isolate the edges in three directions and thus reduce the annoying interdirectional interference in the resolution enhancement process. Although a number of DWT-based interpolation methods[7,24,26,27] have been developed for preserving the missing high-frequency components of the given LR image, the blurring effect from their employed interpolation methods causes the potential loss of edges in these subbands. For example, bicubic, the most widely used interpolation method in wavelet-based resolution enhancement approaches, can produce blurring around edge areas because of the smoothing process. Therefore, the blurring effect caused by the interpolation method needs to be addressed.

Many DT-CWT-based resolution enhancement methods[33–35] attempt to address this problem. In Ref. 33, EDI[13] was employed as an alternative interpolation method of high-frequency subbands obtained by DT-CWT. Later, Izadpanahi and Demirel[34] proposed an extended version of this approach for multiframe SR. Recently, the same authors applied NEDI,[14] which improved the performance of EDI, for the interpolation of high-frequency subbands generated by DT-CWT for motion-based video SR.[35] In this work, NEDI is employed to process the high-frequency subbands obtained through DWT and output the interpolated subbands using a nonlinear adaptive threshold.

This paper proposes combining DWT and NEDI, which integrates merits from both the frequency domain and spatial domain and substantially improves the visual quality of the pixels around edges. The advantage of using DWT with NEDI is it recovers the edge details of directional high-frequency subbands and thus decreases the undesirable interdirectional interference in the SR process. This merit cannot be achieved using only the NEDI method. Consider an input LR image with the size of $W \times H$, and the scale factor is denoted by $\alpha$. Initially, one-level DWT process decomposes the input LR image into four frequency subbands, called low-high (LH), high-low (HL), and high-high (HH) respectively. Each subband has half of the size of the input image due to downsampling. The high-frequency subbands (LH, HL, and HH) are interpolated using the NEDI method with the scale factor $\alpha$. Generally, data sets recorded by sensors are most commonly corrupted by noise, such as additive Gaussian noise and multiplicative noise. Therefore, to preserve more edges and reduce the noise in the estimated high-frequency subbands, a thresholding procedure using an adaptive threshold is included to process the produced wavelet coefficients. Many types of thresholding functions have been introduced for the modification of estimated wavelet coefficients, such as hard, soft, semisoft, and garrote.[36] This paper employs a soft-thresholding technique proposed by Donoho[37] and extended by Zhang.[38] The universal threshold $\tau$ for the considered subband can be calculated as

$$\tau = \sigma\sqrt{2\ \log(N)/N}, \tag{1}$$

where $\sigma$ is the standard deviation of the subband and $N$ is the total number of pixels. The nonlinear soft-thresholding function is defined as

$$X_{\text{out}}(i,j) = \begin{cases} X_{\text{in}}(i,j) - \tau & X_{\text{in}}(i,j) > \tau \\ 0 & |X_{\text{in}}(i,j)| \le \tau \\ X_{\text{in}}(i,j) + \tau & X_{\text{in}}(i,j) < -\tau \end{cases}. \tag{2}$$

The basic idea of this thresholding process is that the energy of a signal is often concentrated on a few coefficients while the energy of noise is spread among all coefficients in the wavelet domains. Therefore, the nonlinear soft-thresholding tends to maintain few larger coefficients representing the signal while reducing noise coefficients to zero in the wavelet domain. A universal threshold is intuitively expected to uniformly remove the noise since the Gaussian noise still has the same variance over different scales in the transform domain.[38] The application of this soft-thresholding function is based on the hypothesis that the large coefficients in the high-frequency subbands reflect the true edges of objects while the small coefficients reflect the noise. This hypothesis can be proven by Fig. 1, where (a) shows the observed LR image and (b) shows the reconstruction image of high-frequency subbands only without thresholding. Both true edges and noise can be observed in Fig. 1(b). Figure 1(c) shows the reconstruction image of high-frequency subbands where the small coefficients are removed. It can be observed that the noise is significantly reduced while the true edges are preserved. The reconstruction image of high-frequency subbands where the large coefficients are removed is illustrated by Fig. 1(d), which is dominated by noise with very little true edge information found.

The input LR image, interpolated by the NEDI method with half of the scale factor $\alpha/2$, is used as the estimated LL subband because it contains more information than the LL subband produced by the DWT process, as suggested in Refs. 7, 24, and 26. Finally, IDWT is applied to achieve a super-resolved image by combining the estimated LL subband and corrected high-frequency subbands. The block diagram of the DWT-NEDI approach is illustrated by Fig. 2.

The proposed approach can be summarized by the following steps:

1. Consider the red channel of the observed LR image.
2. Compute one-level DWT decomposition of this channel.

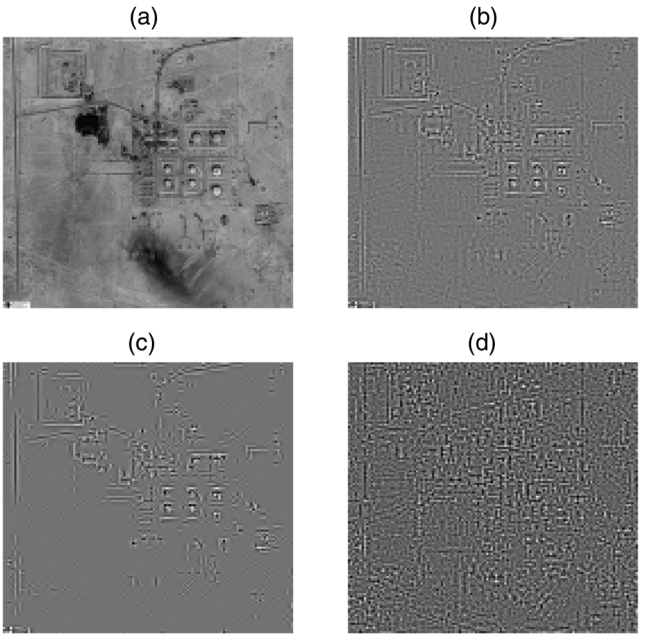


**Fig. 1** An example to help justify the use of thresholding process: (a) the observed LR image, (b) the reconstruction image of high-frequency subbands only without thresholding, (c) the reconstruction image of high-frequency subbands where the small coefficients are removed, and (d) the reconstruction image of high-frequency subbands where the large coefficients are removed.

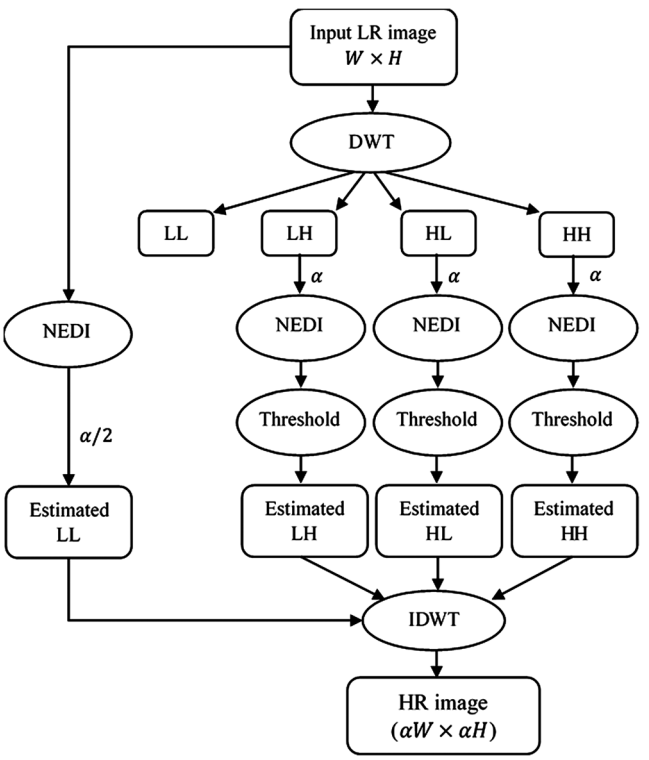


**Fig. 2** Block diagram of the proposed DWT-NEDI resolution enhancement approach.

3. Apply the NEDI method to LH, HL, and HH high-frequency subbands with the scale factor $\alpha$.
4. For each high-frequency subband, calculate the threshold $\tau$.
5. Apply the adaptive thresholding process for each high-frequency subband and create the estimated $\hat{\text{LH}}$, $\hat{\text{HL}}$, and $\hat{\text{HH}}$.
6. Apply the NEDI method to the input LR image with the scale factor $\alpha/2$ to create $\hat{\text{LL}}$.;
7. Apply IDWT using $(\hat{\text{LL}}, \hat{\text{LH}}, \hat{\text{HL}}, \hat{\text{HH}})$ to produce the enhanced channel.
8. Repeat steps 2 to 7 for the blue and green channels.
9. Combine the three enhanced channels into the final enhanced HR color image.

## 3 Results and Discussions

### 3.1 *Visual Evaluation*

The proposed technique was tested on 20 different satellite images obtained from the Satellite Imaging Corporation webpage,[39] which is a public data set. To assess the variation in performance in terms of different types of images, the studied satellite images were divided into five classes: "natural disaster, tourism, defence and intelligence, construction, and cadastre and land." Each class includes four images that were randomly selected from the data set. The size of the original HR images in the public data set is different. For the consistency of comparison, each original HR image was therefore resized to $512 \times 512$ pixels as the reference image. The input LR images with the size of $128 \times 128$ pixels were produced from blurring and downsampling the original HR images by applying twice cascaded DWT with the db.9/7 wavelet filter. The LR images are further corrupted by a Gaussian noise with the signal-to-noise ratio (SNR) of 40 dB. The biorthogonal Daubechies (db.9/7) was chosen because the literature review shows that it is the most commonly used wavelet function for the decomposition process by DWT.[40] Note that all methods, including the proposed method and other considered methods, were implemented by the authors using MATLAB® 2015.

To demonstrate the visual quality of the produced results, one image was randomly selected from four groups and tested by the proposed technique. Figures 3 and 4 show the super-resolved images using the proposed technique and the other considered methods with an enlargement from $128 \times 128$ to $512 \times 512$ of the images from the construction and tourism groups. The visual results demonstrate the ability of the DWT-NEDI technique to enhance the observed LR images by proving more sharp edges, potentially offering more details of interested objects.

### 3.2 *Quantitative Evaluation*

The difference between the super-resolved images from different techniques can be small, and it is difficult to be inspected visually. This section presents the results of quantitative comparison. The peak-SNR (PSNR) between the super-resolved image and the original HR image is one of the most commonly used objective fidelity criteria for evaluating image quality. It can be calculated as

$$\text{PSNR} = 10 \log_{10}\left(\frac{L^2}{\text{MSE}}\right), \tag{3}$$

where $L$ is the maximum fluctuation in the image. If the image is represented by 8-bit grayscale, the value of $L$

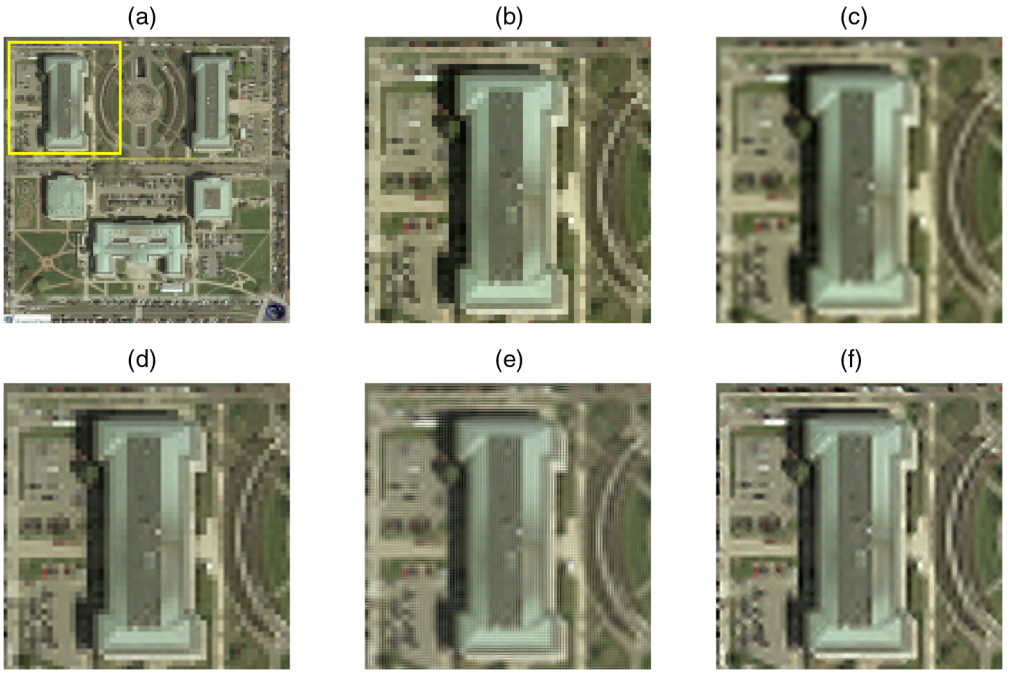


**Fig. 3** Resolution enhanced results from the proposed approach with an enlargement from $128 \times 128$ to $512 \times 512$ for an image selected from the construction group: (a) the whole input LR image; (b) the selected region of the input LR image; super-resolved HR images by (c) bicubic, (d) WZP, (e) DASR, and (f) the proposed method.

will be 255. MSE represents the mean-square-error between the super-resolved image $\hat{X}(i,j)$ and the original HR image $X(i,j)$. It can be calculated as

$$\mathrm{MSE} = \frac{1}{W \times H} \sum_{i=1}^{W} \sum_{j=1}^{H} [\hat{X}(i,j) - X(i,j)]^2. \quad (4)$$

The root-mean-square error (RMSE) between these two images is also one of the commonly used quantitative measures,[12] and it can be expressed as

$$\mathrm{RMSE} = \sqrt{\mathrm{MSE}}. \quad (5)$$

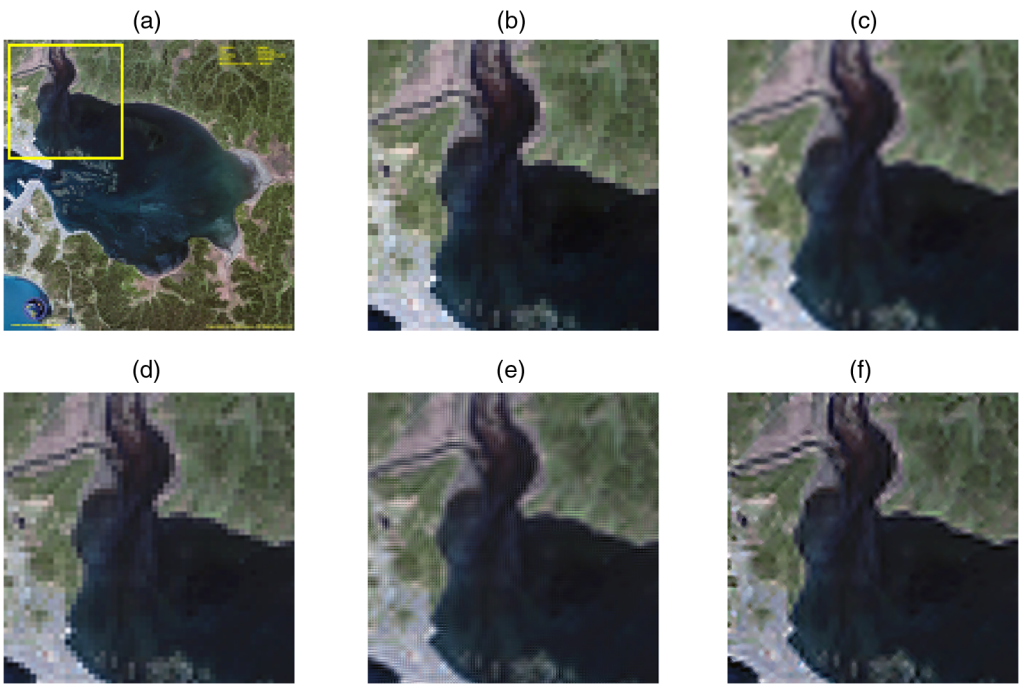


**Fig. 4** Resolution enhanced results from the proposed approach with an enlargement from $128 \times 128$ to $512 \times 512$ for an image selected from the tourism group: (a) the whole input LR image; (b) the selected region of the input LR image; resolution enhanced images by (c) bicubic, (d) WZP, (e) DASR, and (f) the proposed method.

Entropy is another quantitative measure used to assess image quality when the error images for different image resolution enhancement techniques are very close to each other and it is very difficult to make assessment. The entropy of a negative error image, denoted by $E$, can be calculated as

$$E = -\sum_{k=1}^{L} P(r_k) \log_2 P(r_k), \tag{6}$$

where $P(r_k)$ is the probability of an intensity value $r_k$. The lower the $E$, the better the improvement is.[41]

To complement the quantitative analysis, the structural similarity (SSIM)[42] image quality measure has also been applied. The SSIM index evaluates the visual effect of three characteristics of an image: luminance, contrast, and structure. It is based on the computation of these three components and is an inner product of them. It is defined as

$$\mathrm{SSIM} = \frac{(2\mu_{\hat{X}}\mu_X + C_1)(2\sigma_{\hat{X}}\sigma_X + C_2)}{(\mu_{\hat{X}}^2 + \mu_X^2 + C_1)(\sigma_{\hat{X}}^2 + \sigma_X^2 + C_2)}, \tag{7}$$

where $\mu_{\hat{X}}$, $\mu_X$ are the local means for the images $\hat{X}$, $X$, respectively, $\sigma_{\hat{X}}$, $\sigma_X$ are corresponding standard deviations, and $C_1$, $C_2$ are two constants used to avoid the instability.

The quantitative performances measured by PSNR, RMSE, entropy, and SSIM for the selected examples of each group are listed in Tables 1–4, respectively. In terms of the results of PSNR and RMSE, the proposed technique has the best performance for all five selected images. In terms of the results of SSIM, the proposed technique and WZP-CS achieve the highest performance for the images from the natural disaster and tourism groups, whereas the proposed technique is the best for the images from the remaining groups. In terms of the values of entropy, the nearest neighbor has the best performance for the images from

**Table 1** PSNR (db) results of the selected images for resolution enhancement from $128 \times 128$ to $512 \times 512$, where the bold values indicate the best performance of each column in terms of PSNR.

| | Image group[a] | | | | |
|---|---|---|---|---|---|
| Techniques | 1 | 2 | 3 | 4 | 5 |
| Nearest | 22.42 | 25.87 | 22.53 | 19.66 | 15.92 |
| Bilinear | 23.25 | 26.67 | 23.21 | 20.42 | 16.65 |
| Bicubic | 23.20 | 26.68 | 23.18 | 20.39 | 16.61 |
| Lanczos | 23.15 | 26.65 | 23.13 | 20.35 | 16.56 |
| WZP | 23.65 | 26.92 | 23.50 | 20.82 | 16.93 |
| WZP-CS | 24.17 | 27.57 | 23.79 | 21.27 | 17.34 |
| DWT | 23.54 | 26.83 | 23.42 | 20.71 | 16.85 |
| DASR | 22.99 | 26.48 | 22.90 | 20.00 | 16.51 |
| DWT-Diff | 21.92 | 25.47 | 21.89 | 18.94 | 15.57 |
| DWT-SWT | 22.31 | 25.87 | 22.37 | 19.43 | 15.99 |
| DWT-NEDI | **24.90** | **27.83** | **24.53** | **21.93** | **18.01** |

[a]Group 1: natural disaster; 2: tourism; 3: defence and intelligence, 4: construction, and 5: cadastre and land.

**Table 2** RMSE results of the selected images for resolution enhancement from $128 \times 128$ to $512 \times 512$, where the bold values indicate the best performance of each column in terms of RMSE.

| | Image group | | | | |
|---|---|---|---|---|---|
| Techniques | 1 | 2 | 3 | 4 | 5 |
| Nearest | 19.31 | 12.98 | 19.06 | 26.51 | 40.80 |
| Bilinear | 17.55 | 11.84 | 17.62 | 24.30 | 37.50 |
| Bicubic | 17.63 | 11.83 | 17.68 | 24.39 | 37.68 |
| Lanczos | 17.74 | 11.87 | 17.78 | 24.51 | 37.91 |
| WZP | 16.75 | 11.50 | 17.04 | 23.20 | 36.30 |
| WZP-CS | 15.77 | 10.67 | 16.49 | 22.03 | 34.63 |
| DWT | 16.96 | 11.61 | 17.20 | 23.50 | 36.64 |
| DASR | 18.08 | 12.10 | 18.26 | 25.50 | 38.11 |
| DWT-Diff | 20.43 | 13.59 | 20.51 | 28.82 | 42.46 |
| DWT-SWT | 19.54 | 12.97 | 19.42 | 27.24 | 40.47 |
| Proposed method | **14.50** | **10.35** | **15.13** | **20.42** | **32.05** |

**Table 3** Entropy results of the selected images for resolution enhancement from $128 \times 128$ to $512 \times 512$, where the bold values indicate the best performance of each column in terms of entropy.

| | Image group | | | | |
|---|---|---|---|---|---|
| Techniques | 1 | 2 | 3 | 4 | 5 |
| Nearest | **5.01** | **4.83** | 5.62 | 5.83 | 6.06 |
| Bilinear | 5.31 | 4.96 | 5.84 | 6.08 | 6.19 |
| Bicubic | 5.21 | 4.92 | 5.82 | 5.92 | 6.15 |
| Lanczos | 5.21 | 4.92 | 5.81 | 5.91 | 6.21 |
| WZP | 5.13 | 4.86 | **5.60** | 5.67 | 5.98 |
| WZP-CS | 5.20 | 4.87 | 5.79 | 5.65 | 6.11 |
| DWT | 5.04 | 4.89 | 5.62 | 5.59 | 5.98 |
| DASR | 5.17 | 4.85 | 5.70 | 5.87 | 6.13 |
| DWT-Diff | 5.20 | 4.86 | 5.71 | 5.71 | **5.88** |
| DWT-SWT | 5.17 | 5.02 | 5.66 | 5.84 | 5.90 |
| Proposed method | 5.16 | 4.89 | 5.83 | **5.54** | 6.14 |

**Table 4** SSIM results of the selected images for resolution enhancement from $128 \times 128$ to $512 \times 512$, where the bold values indicate the best performance of each column in terms of SSIM.

| Techniques | Image group | | | | |
|---|---|---|---|---|---|
| | 1 | 2 | 3 | 4 | 5 |
| Nearest | 0.27 | 0.26 | 0.21 | 0.24 | 0.17 |
| Bilinear | 0.31 | 0.29 | 0.21 | 0.26 | 0.19 |
| Bicubic | 0.33 | 0.31 | 0.23 | 0.28 | 0.21 |
| Lanczos | 0.33 | 0.31 | 0.24 | 0.28 | 0.21 |
| WZP | 0.34 | 0.34 | 0.29 | 0.33 | 0.25 |
| WZP-CS | **0.38** | **0.37** | 0.30 | 0.35 | 0.27 |
| DWT | 0.33 | 0.33 | 0.28 | 0.32 | 0.25 |
| DASR | 0.31 | 0.30 | 0.24 | 0.26 | 0.22 |
| DWT-Diff | 0.25 | 0.25 | 0.21 | 0.23 | 0.19 |
| DWT-SWT | 0.28 | 0.27 | 0.22 | 0.24 | 0.20 |
| Proposed method | **0.38** | 0.36 | **0.32** | **0.37** | **0.28** |

the natural disaster and tourism groups, WZP and DWT-Diff produces the highest performance for the images from the defence and cadastre groups, while the proposed technique is the best for the images from the construction group.

The above four criteria can be used to compare the performances of different techniques for a single image. However, they are not straightforward for collectively evaluating the performance for a number of testing images. This paper proposes four normalized criteria to better measure the improved performance of a considered resolution enhancement technique compared with a reference technique, which includes ratio of PSNR (RPSNR), ratio of RMSE (RRMSE), ratio of entropy (RENTROPY), and ratio of SSIM (RSSIM). They can be calculated as

$$\mathrm{RPSNR}(m_1, m_2) = \frac{\mathrm{PSNR}(m_1) - \mathrm{PSNR}(m_2)}{\mathrm{PSNR}(m_2)} \times 100\%, \quad (8)$$

$$\mathrm{RRMSE}(m_1, m_2) = \frac{\mathrm{RMSE}(m_1) - \mathrm{RMSR}(m_2)}{\mathrm{RMSE}(m_2)} \times 100\%, \quad (9)$$

$$\mathrm{RENTROPY}(m_1, m_2) = \frac{E(m_1) - E(m_2)}{E(m_2)} \times 100\%, \quad (10)$$

$$\mathrm{RSSIM}(m_1, m_2) = \frac{\mathrm{PSNR}(m_1) - \mathrm{PSNR}(m_2)}{\mathrm{PSNR}(m_2)} \times 100\%, \quad (11)$$

where $m_1$ is the considered resolution enhancement technique and $m_2$ is the reference technique, which was chosen as the bicubic interpolation method in this paper due to its popularity. The higher the RPSNR and RSSIM, the better the performance of the considered technique is. A positive value of RPSNR indicates a better performance than the reference

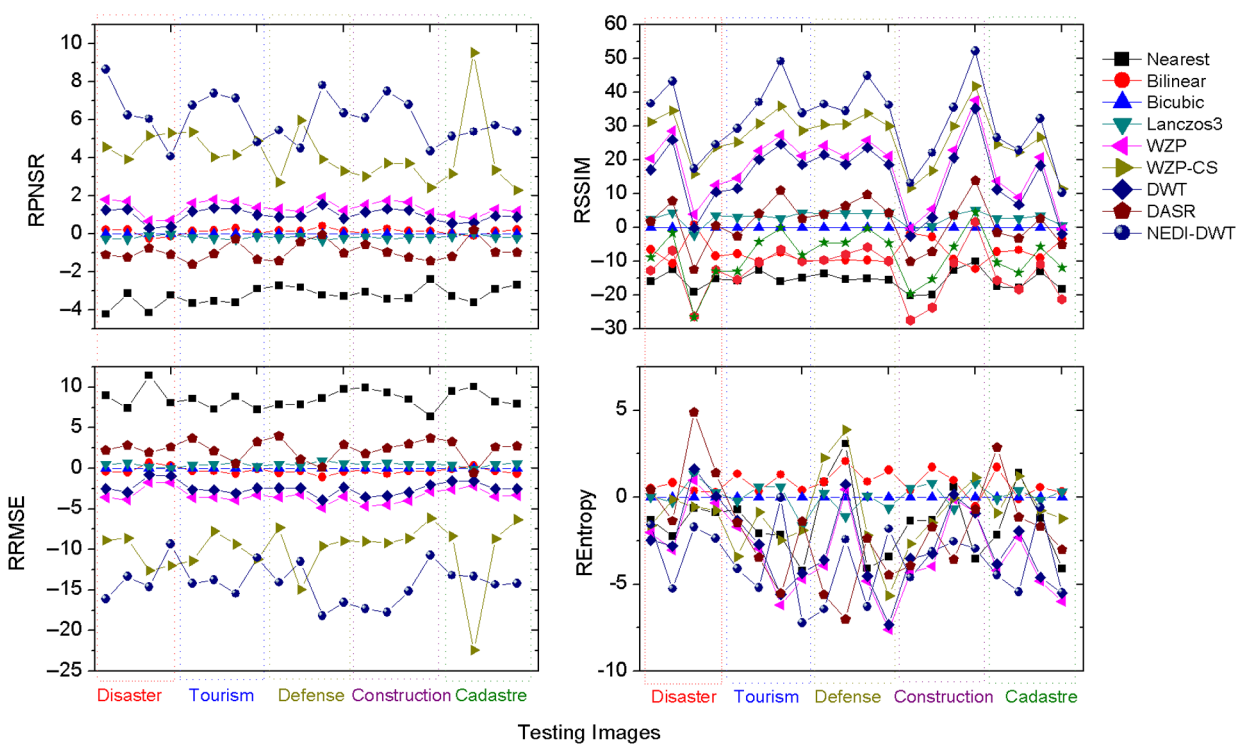


**Fig. 5** Comparison of RPSNR, RRMSE, RSSIM, and RENTROPY results of all tested images for resolution enhancement from $128 \times 128$ to $512 \times 512$ by the proposed approach and the conventional and state-of-the-art resolution enhancement techniques.

method. The lower the RRMSE and RENTROPY, the better the performance of the considered technique is. A negative value of RRMSE and RENTROPY indicates a better performance than the reference method.

Figure 5 shows the results of the proposed criteria for all 20 testing images, organized by five groups, using the selected nine resolution enhancement techniques, which include the nearest neighbor, the bilinear interpolation, the bicubic interpolation, the Lanczos interpolation, WZP, WZP-CS, DWT, DASR, and the proposed technique. The wavelet function db.9/7 was used in the wavelet-based techniques. To evaluate the overall performance of the proposed technique for different classes of satellite images, Table 5 shows the percentage of images in which the DWT-NEDI technique has the best performance among the considered techniques. It can be inferred from Fig. 5 that the DWT-NEDI technique has superior performance against other methods in terms of RPSNR and RRMSE, which is supported by it topping the performance for 80% of images, especially for the image from the construction group in which it tops 100%. In terms of RSSIM, it tops the performance for 100% of all images from five groups. For the remaining 20% of images, the WZP-CS has the best performance. However, in terms of RENROPY, the difference of performance is not significant among the considered methods. On average, the DWT-NEDI technique still has the best performance as it tops 60% of images.

### 3.3 *Variation of Wavelet Functions*

All above results from the wavelet-based resolution enhancement techniques were produced by the most widely used wavelet function db.9/7. This section discusses the prospect of the proposed approach using other wavelet functions. Previous research shows that the selection of wavelet function can affect the performance.[43] A total of 50 wavelet functions, including db.1-20, sym.2-20, bior.1-6, and coif.1-5,[44] were tested using the proposed technique. Table 6 shows the calculated PSNR results for randomly selected satellite images from each group using nine wavelet functions, which include db1, db2, sym16, sym20, ciof1, ciof2, db.9/7, bior5.5, and bior6.8 as well as bicubic interpolation. These functions were selected due to their better performance than the remaining functions. The patterns for five groups of images are very similar; for example, (a) the performance of the proposed technique using the selected wavelet functions is better than the bicubic interpolation; (b) the function db.9/7 has relatively high PSNR and is in the top 3; and (c) the function bior5.5 has the highest PSNR value, although its superiority over db.9/7 is relatively small.

**Table 5** Percentage of tested images in which the proposed technique tops the performance.

| Image group | RPSNR (%) | RRMSE (%) | RENTROPY (%) | RSSIM (%) |
|---|---|---|---|---|
| Natural disaster | 75 | 75 | 75 | 100 |
| Tourism | 75 | 75 | 75 | 100 |
| Defence and intelligence | 75 | 75 | 50 | 100 |
| Construction | 100 | 100 | 50 | 100 |
| Cadastre and land | 75 | 75 | 75 | 100 |
| Average | 80 | 80 | 65 | 100 |

**Table 6** PSNR values produced by the proposed approach using the selected wavelet functions for randomly selected images from each group, where top three are highlighted in bold.

| Wavelet functions | Natural disaster | Tourism | Defence | Construction | Cadastre and land |
|---|---|---|---|---|---|
| bicubic | 28.49 | 24.66 | 24.13 | 20.09 | 17.33 |
| db1 | 29.99 | 25.67 | 25.16 | 21.26 | 18.45 |
| db2 | 30.43 | 25.99 | 25.43 | 21.56 | 18.76 |
| sym16 | 30.60 | **26.15** | 25.56 | **21.74** | **18.90** |
| sym20 | 30.60 | **26.15** | 25.56 | **21.74** | **18.90** |
| ciof1 | 30.57 | 26.11 | 25.52 | 21.69 | 18.86 |
| ciof2 | 29.47 | 25.26 | 24.80 | 20.78 | 18.06 |
| db.9/7 | **30.70** | **26.24** | **25.63** | **21.82** | **19.00** |
| bior5.5 | **30.74** | **26.30** | **25.69** | **21.88** | **19.05** |
| bior6.8 | **30.61** | 26.14 | **25.56** | 21.73 | **18.90** |

## 4 Conclusions

A resolution enhancement approach based on DWT and NEDI was proposed in this paper to correct the errors in image geometry and recover the details of directional high-frequency subbands. A nonlinear adaptive thresholding process is also included to boost the edges and reduce the noise in the estimated high-frequency subbands for enhancing satellite images. The motivation for this approach is to better preserve the edges and remove potential noise in the estimated high-frequency subbands since a direct interpolation through interpolation methods will blur the areas around edges. Five groups of satellite images (totally 20 images), randomly selected from a public data set, were tested by the proposed approach, and the results were compared with the conventional interpolation methods and state-of-the-art techniques. Four criteria were introduced to better evaluate the overall performance of the proposed technique for multiple images. Results show that the proposed method outperforms conventional image interpolation approaches, in both objective and subjective terms, and in most scenarios it also outperforms the state-of-the-art methods operating in the wavelet domain.

Future work will focus on the employment of other advanced decomposition approaches, such as curvelet, contourlet, and Shearlet transform, to further improve the performance.

## *References*

1. M. S. Divya Lakshmi, "Robust satellite image resolution enhancement based on interpolation of stationary wavelet transform," *Int. J. Sci. Eng. Res.* **4**(6), 1365 (2013).

2. J. Tian and K.-K. Ma, "A survey on super-resolution imaging," *Signal Image Video Process.* **5**(3), 329–342 (2011).
3. S. C. Park, M. K. Park, and M. G. Kang, "Super-resolution image reconstruction: a technical overview," *IEEE Signal Process Mag.* **20**(3), 21–36 (2003).
4. J. A. Richards and X. Jia, *Remote Sensing Digital Image Analysis: An Introduction*, 5th ed., Springer, Berlin (2013).
5. S. M. De Jong and F. D. Van Der Meer, *Remote Sensing Image Analysis: Including the Spatial Domain*, Springer, Dordrecht (2004).
6. H. Demirel and G. Anbarjafari, "Satellite image resolution enhancement using complex wavelet transform," *IEEE Geosci. Remote Sens. Lett.* **7**(1), 123–126 (2010).
7. H. Demirel and G. Anbarjafari, "Discrete wavelet transform-based satellite image resolution enhancement," *IEEE Trans. Geosci. Remote Sens.* **49**(6), 1997–2004 (2011).
8. M. Z. Iqbal, A. Ghafoor, and A. M. Siddiqui, "Satellite image resolution enhancement using dual-tree complex wavelet transform and nonlocal means," *IEEE Geosci. Remote Sens. Lett.* **10**(3), 451–455 (2013).
9. F. S. Robinson et al., "Novel applications of super-resolution in medical imaging," in *Super-Resolution Imaging*, P. Milanfar, Ed., pp. 383–412, CRC Press, Boca Raton, Florida (2010).
10. H. Greenspan, "Super-resolution in medical imaging," *Comput. J.* **52**(1), 43–63 (2008).
11. L. Zhang et al., "A super-resolution reconstruction algorithm for surveillance images," *Signal Process.* **90**(3), 848–859 (2010).
12. R. C. Gonzalez and R. E. Woods, *Digital Image Processing*, Prentice Hall, Englewood Cliffs, New Jersey (2007).
13. J. Allebach and P. W. Wong, "Edge-directed interpolation," in *Proc. of 3rd IEEE Int. Conf. on Image Processing*, Vol. 3, pp. 707–710 (1996).
14. X. Li and M. T. Orchard, "New edge-directed interpolation," *IEEE Trans. Image Process.* **10**(10), 1521–1527 (2001).
15. W.-S. Tam, C.-W. Kok, and W.-C. Siu, "A modified edge directed interpolation for images," *J. Electron. Imaging* **19**(1), 013011 (2010).
16. S. Izadpanahi and H. Demirel, "Motion block based video super resolution," *Digital Signal Process.* **23**(5), 1451–1462 (2013).
17. S. G. Chang, Z. Cvetkovic, and M. Vetterli, "Resolution enhancement of images using wavelet transform extrema extrapolation," in *Int. Conf. on Acoustics, Speech, and Signal Processing (ICASSP'95)*, Vol. 4, pp. 2379–2382 (1995).
18. W. K. Carey, D. B. Chuang, and S. S. Hemami, "Regularity-preserving image interpolation," *IEEE Trans. Image Process.* **8**(9), 1293–1297 (1999).
19. K. Kinebuchi, D. D. Muresan, and T. W. Parks, "Image interpolation using wavelet based hidden Markov trees," in *IEEE Int. Conf. on Acoustics, Speech, and Signal Processing. Proc. (ICASSP'01)*, Vol. 3, pp. 1957–1960 (2001).
20. S. Zhao, H. Han, and S. Peng, "Wavelet-domain HMT-based image super-resolution," in *Proc. Int. Conf. on Image Processing (ICIP'03)*, Vol. 3, pp. II–953–6 (2003).
21. A. Temizel and T. Vlachos, "Wavelet domain image resolution enhancement using cycle-spinning," *Electron. Lett.* **41**(3), 119 (2005).
22. T. Vlachos, "Image resolution upscaling in the wavelet domain using directional cycle spinning," *J. Electron. Imaging* **14**(4), 040501 (2005).
23. A. Temizel and T. Vlachos, "Wavelet domain image resolution enhancement using cycle spinning and edge modelling," in *13th European Signal Processing Conf.*, pp. 1–4 (2005).
24. T. Acharya and P.-S. Tsai, "Edge enhanced image up-sampling algorithm using discrete wavelet transform," US 6377280 B1 (2002).
25. P.-S. Tsai and T. Acharya, "Image up-sampling using discrete wavelet transform," in *Proc. of the 9th Joint Conf. on Information Sciences (JCIS'06)* (2006).
26. G. Anbarjafari and H. Demirel, "Image super resolution based on interpolation of wavelet domain high frequency subbands and the spatial domain input image," *ETRI J.* **32**(3), 390–394 (2010).
27. H. Demirel and G. Anbarjafari, "IMAGE resolution enhancement by using discrete and stationary wavelet decomposition," *IEEE Trans. Image Process.* **20**(5), 1458–1460 (2011).
28. R. Timofte, V. De Smet, and L. Van Gool, "Anchored neighborhood regression for fast example-based super-resolution," in *Proc., IEEE Int. Conf. on Computer Vision (ICCV'13)*, pp. 1920–1927 (2013).
29. R. Timofte, V. De Smet, and L. Van Gool, "A+: adjusted anchored neighborhood regression for fast super-resolution," in *Proc., IEEE Asian Conf. on Computer Vision (ACCV'14)* (2014).
30. J.-J. Huang and W.-C. Siu, "Learning hierarchical decision trees for single image super-resolution," *IEEE Trans. Circuits Syst. Video Technol.* PP(99), 1–8 (2015).
31. C. Dong et al., "Image super-resolution using deep convolutional networks," *IEEE Trans. Pattern Anal. Mach. Intell.* **38**(2), 295–307 (2016).
32. W. Yang et al., "Deep edge guided recurrent residual learning for image super-resolution," *Comput. Vision Pattern Recognit.* arXiv:1701.05652 (2017).
33. P. Jagadeesh and J. Pragatheeswaran, "Image resolution enhancement based on edge directed interpolation using dual tree complex wavelet transform," in *IEEE Int. Conf. on Recent Trends in Information Technology (ICRTIT'11)* (2011).
34. S. Izadpanahi and H. Demirel, "Multi-frame super resolution using edge directed interpolation and complex wavelet transform," in *IET Conf. on Image Processing (IPR'12)*, pp. 1–5, IET (2012).
35. S. Izadpanahi and H. Demirel, "Motion based video super resolution using edge directed interpolation and complex wavelet transform," *Signal Process.* **93**(7), 2076–2086 (2013).
36. A. K. Bhandari et al., "Cuckoo search algorithm based satellite image contrast and brightness enhancement using DWT–SVD," *ISA Trans.* **53**(4), 1286–1296 (2014).
37. D. L. Donoho, "De-noising by soft-thresholding," *IEEE Trans. Inf. Theory* **41**(3), 613–627 (1995).
38. X.-P. Zhang, "Thresholding neural network for adaptive noise reduction," *IEEE Trans. Neural Networks* **12**(3), 567–584 (2001).
39. Satellite Imaging Corporation, "Satellite image gallery," http://www.satimagingcorp.com/gallery/ (1 April 2015).
40. A. Skodras, C. Christopoulos, and T. Ebrahimi, "The JPEG 2000 still image compression standard," *IEEE Signal Process Mag.* **18**(5), 36–58 (2001).
41. S. Azam, F. T. Zohra, and M. M. Islam, "A state-of-the-art review on wavelet based image resolution enhancement techniques: performance evaluation criteria and issues," *Int. J. Image Graphics Signal Process.* **6**(9), 35–46 (2014).
42. Z. Wang et al., "Image quality assessment: from error visibility structural similarity," *IEEE Trans. Image Process.* **13**(4), 600–612 (2004).
43. W. Witwit et al., "An optimal factor analysis approach to improve the wavelet-based image resolution enhancement techniques," *Global J. Comput. Sci. Technol.* **16**(3), 11–20 (2016).
44. R. C. Gonzalez and R. E. Woods, *Digital Image Processing Using MATLAB*, Prentice Hall, Englewood Cliffs, New Jersey (2004).



**Wasnaa Witwit** is currently pursuing her PhD at Cranfield University, United Kingdom. She worked as a research assistant at the Department of Physics of Babylon University, Iraq. She received her MSc degree in resampling of astronomical images from the University of Babylon in 2002. Her research interests are in image processing, astronomical and satellite images analysis, interpolation, and video super-resolution.

**Yifan Zhao** is a lecturer of image and signal processing and degradation assessment at Cranfield University. He received his PhD in automatic control and system engineering from the University of Sheffield in 2007. He received his MSc and BEng degrees in automatic control theory and engineering from Beijing Institute of Technology, China, in 2003 and 2000, respectively. His current research interests are computer vision, super-resolution, thermography for nondestructive testing, and electroencephalogram data analysis.

**Karl Jenkins** received his PhD in wave modeling from the University of Manchester in 1996. Currently, he is the head of the Centre for Computational Engineering Sciences at Cranfield University. He is also the program director for his MSc degree in computational and software techniques in engineering with specialist option in digital signal and image processing. His current research interests are computational engineering, high fidelity computational fluid dynamics simulations, and high performance.

**Yitian Zhao** is a lecturer at the Beijing Institute of Technology, China. He obtained his PhD in computer science from Aberystwyth University, United Kingdom, in 2013. From November of 2013 to October 2014, he worked as a research assistant at the University of Liverpool. His primary research interests lie in 2-D/3-D image processing, medical image analysis, pattern recognition, computer graphics, and data- and knowledge-base systems.